metals

MDPI

Article

Microstructure, Mechanical Properties, and Fatigue Fracture Characteristics of High-Fracture-Resistance Selective Laser Melting Al-Ni-Cu Alloys

Kai-Chieh Chang, Jun-Ren Zhao and Fei-Yi Hung *

Department of Materials Science and Engineering, National Cheng Kung University, Tainan 701, Taiwan; eran871003@gmail.com (K.-C.C.); a2x346yz03@gmail.com (J.-R.Z.)

* Correspondence: fyhung@mail.ncku.edu.tw; Tel.: +886-6-275-7575 (ext. 62950)

Abstract: Al-Ni-Cu alloys are used in energy, automotive, and aerospace industries because of their excellent mechanical properties, corrosion resistance, and high-temperature stability. In this study, Al-Ni-Cu alloy powder was subjected to selective laser melting (SLM). The SLM Al-Ni-Cu alloy was manufactured using appropriate printing parameters, and its properties were investigated. The results revealed that the As-printed material exhibited a typical melting pool stack structure, with an ultimate tensile strength of 725 MPa but a high brittleness effect (low ductility). After traditional heat treatment, the melting pool structure did not completely disappear. The strengthening phase $Al_7Cu_{23}Ni$ precipitated from the boundary of the melting pools; thus, the Al-Ni-Cu alloy maintained high strength (>500 MPa) and considerably increased ductility (>10%). The SLM Al-Ni-Cu alloy has considerable industrial application potential; therefore, increasing the heat treatment temperature or extending the heat treatment time in the future works can promote the decomposition of the melting pool boundary and solve the problem related to the aggregation behavior of the precipitation phase, thereby improving the fatigue life of the alloy.

Keywords: Al-Ni-Cu; selective laser melting; heat treatment; tensile properties; fatigue

Citation: Chang, K.-C.; Zhao, J.-R.; Hung, F.-Y. Microstructure, Mechanical Properties, and Fatigue Fracture Characteristics of High-Fracture-Resistance Selective Laser Melting Al-Ni-Cu Alloys. *Metals* **2021**, *11*, 87. https://doi.org/10.3390/met11010087

Received: 16 December 2020
Accepted: 31 December 2020
Published: 4 January 2021

1. Introduction

The Al-Ni-Cu alloy is a novel aluminum alloy that is often used in the automotive, energy, and aerospace industries because its Al_3Ni eutectic phase exhibits excellent thermal stability [1–3]. The mechanical properties of Al-Ni alloys in the conventional casting process are poor due to casting segregation. However, studies have indicated that the mechanical properties of Al-Ni alloys can be improved through heat treatment [3–9]. Suwanpreecha et al. [3] doped up to 0.4 wt.% Sc in the cast Al-Ni alloy to improve the hardness and high-temperature stability without destroying the eutectic structure. Peng et al. [9] revealed that directional solidification effectively improves the tensile strength and elongation of the aforementioned alloy. The limited mechanical properties of Al-Ni alloys inhibit their application. Therefore, in this study, Cu was added to an Ai-Ni alloy to form Al-Ni-Cu alloy powder and the additive manufacturing method was used to investigate the structural characteristics and destruction resistance of the Al-Ni-Cu alloy.

The selective laser melting (SLM) process used in this study is additive manufacturing technology. In the SLM process, high-power laser selective scanning is used to melt metal powder. Subsequently, rapid solidification is conducted with a high cooling rate to ensure adherence to the previous layer [10–12]. The SLM process exhibits the advantages of cost-effective mold development, the manufacturing of complex geometric shapes, customization, and high dimensional accuracy [12–15]. The SLM process is typically applied to aluminum alloys, such as Al-Si-Mg [12,16–18], Al-Mg-Sc-Zr [19–21], and 7075 aluminum alloys [22,23]. Al-Ni alloys exhibit excellent fluidity [3] and are suitable for the SLM process. In addition, the SLM process is also widely used in titanium-based

and nickel-based alloys [10,11,13–15,24–26]. However, limited studies have been conducted on SLM Al-Ni alloys. Boussinot et al. [27] reported the eutectic microstructure of SLM Al-Ni alloys changes when adjusting the nickel concentration and solidification rate. No relevant study has reported on SLM Al-Ni-Cu alloys. Some reports have indicated that heat treatment can improve the mechanical properties of SLM aluminum alloys. Churyumov et al. [28] revealed that annealed SLM Al-Mg-Sc alloys exhibit excellent strength and ductility. Knoop et al. [29] revealed that aging treatment parameters considerably affect the tensile strength of SLM Al-Si-Mg alloys.

Therefore, this study applied the solid solution and aging heat treatment conditions of typical aluminum alloys to an SLM Al-Ni-Cu alloy to improve the brittleness effect of the SLM Al-Ni-Cu alloy (low elongation) and to investigate its microstructure, tensile mechanical properties, and fatigue failure characteristics before and after heat treatment. Studies of the mechanical properties and fatigue failure mechanism of SLM Al-Ni-Cu alloy are currently quite rare. Furthermore, the SLM Al-Ni-Cu alloy with high fracture resistance has considerable potential in the aerospace field. The establishment of aforementioned information is critical for SLM Al-Ni-Cu alloy industrial application. The results revealed that conventional treatment conditions of aluminum alloys are unsuitable for SLM Al-Ni-Cu alloys and that the fatigue failure characteristics can provide references for SLM industrial applications.

2. Experimental Procedure

An SLM Al-Ni-Cu alloy was manufactured in the study. The printing parameters and chemical composition are listed in Tables 1 and 2, respectively. The printing parameters of this study are referred to in Chen's article [13]. The main additives were 3.8–4.2 and 1.9–2.2 wt.% nickel and copper, respectively. Furthermore, other elements were added to the alloy in small quantities. The average particle size of the powder was 35 μm (powder manufactured by electrode induction-melting inert gas atomization, EIGA, provided by Taiwan Circle Metal Powder Co., as displayed in Figure 1). X-ray diffraction (XRD) analysis indicated that in addition to the aluminum matrix, the alloy powder contained $Al_7Cu_{23}Ni$, $AlCu_3$, and Al_3Ni. The manufacturing direction and the dimensions of the tensile and fatigue specimens are illustrated in Figure 2a–c. The BD (building direction) was perpendicular to the incident laser beam, and the SD (side direction) was parallel to the incident laser beam. After printing, the specimen was removed from the support table through electrical-discharge-machining wire cutting, as displayed in Figure 2d. To speed up the experiments, the diameter of the fatigue test pieces was limited to 6 mm. Additionally, for the purpose of simulating real applications and reducing stress concentration, cylindrical specimens were used.

Table 1. Parameters of the selective laser melting (SLM) process.

Laser Power	Scanning Speed	Beam Size	Hatch Space	Layer Thickness
300 W	700 mm/s	35 μm	100 μm	30 μm

Table 2. Composition of the SLM Al-Ni-Cu alloy powder.

Element	Al	Ni	Cu	Fe	Mn	Zr	Cr	Sc
wt.%	Balance	3.8–4.2	1.9–2.2	1.2–1.5	0.6–0.8	0.6–0.8	0.45–0.55	0.12–0.2
Element	**Si**	**Mg**	**Zn**	**Ti**	**Sn**	**V**	**Be**	**Pb**
wt.%	≤0.1	≤0.05	≤0.05	≤0.05	≤0.05	≤0.05	≤0.05	≤0.05

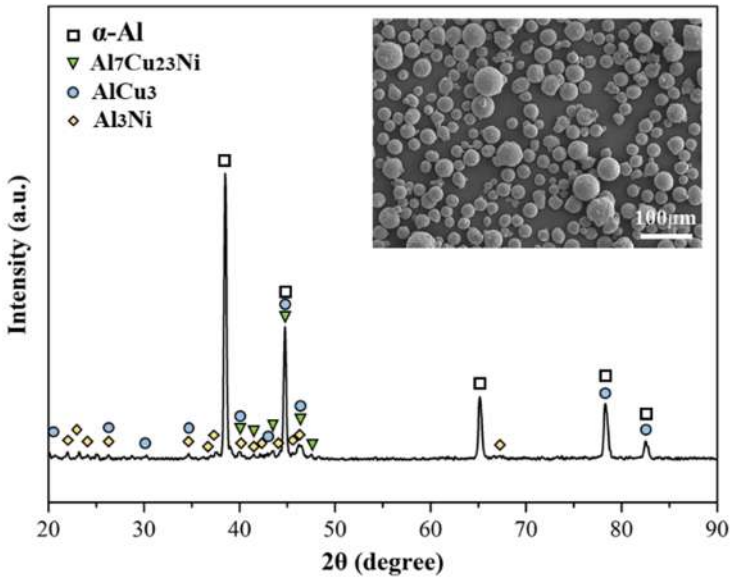

Figure 1. SEM and XRD analysis of the Al-Ni-Cu alloy powders.

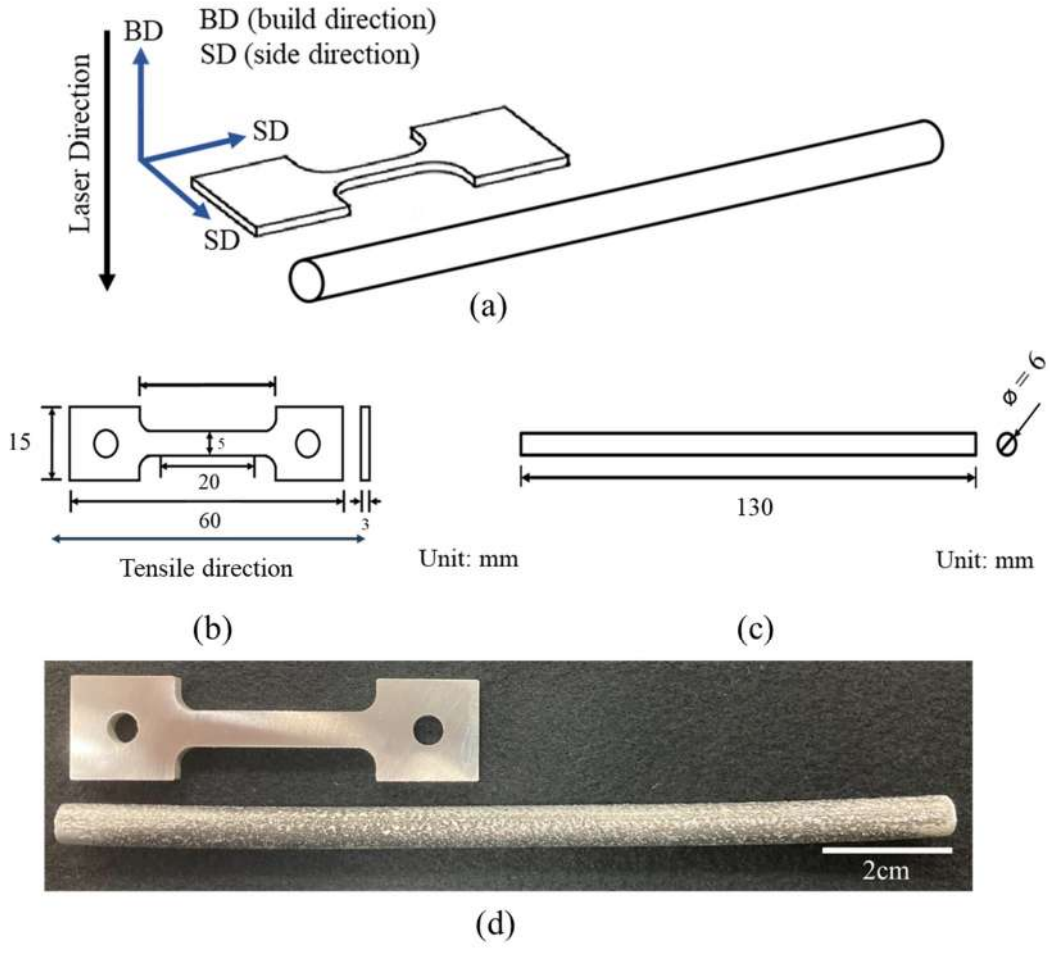

Figure 2. Schematic of the specimen of the Al-Ni-Cu alloy: (**a**) manufacturing direction, (**b**) tensile specimen, (**c**) fatigue specimen, and (**d**) macroscopic morphology photographs.

The SLM Al-Ni-Cu alloy is named the As-printed alloy. The original specimen was subjected to traditional T6 heat treatment [30–33], which involved solution heat treatment at 530 °C for 1 h, followed by water quenching. Next, the specimen was subjected to aging

heat treatment for 2, 4, or 6 h to enhance the precipitation strength of the SLM Al-Ni-Cu alloy. The failure resistance of the specimen before and after heat treatment was compared. Table 3 presents the specimen codes for various heat treatments.

Table 3. Heat treatment parameters of the Al-Ni-Cu alloy before and after solution treatment.

A	As-printed
B	530 °C for 1 h
C	530 °C for 1 h and 175 °C for 2 h
D	530 °C for 1 h and 175 °C for 4 h
E	530 °C for 1 h and 175 °C for 6 h

The specimen was first polished with #80 to #5000 SiC sandpaper in sequence, followed by polishing with 1 and 0.3 μm Al_2O_3 particles and 0.04 μm SiO_2 particles in sequence. Finally, etching was performed by using the Keller's reagent (5 mL HNO_3 + 3 mL HCl + 2 mL HF + 190 mL H_2O). The microstructure was observed through optical microscopy (OM; OLYMPUS BX41M-LED, Tokyo, Japan), and the phase composition was analyzed through XRD (Bruker AXS GmbH, Karlsruhe, Germany).

A universal testing machine (HT-8336, Hung Ta, Taichung, Taiwan) was used for the tensile test. The crosshead speed at 1 mm/min, which correspondeds to the initial strain rate of 18.33×10^{-4} s^{-1}, was used to investigate the effects of heat treatment on the mechanical properties of the Al-Ni-Cu alloy. There are 3–5 samples for each test; the mean value for these samples was taken as the tensile results.

Finally, a rotating fatigue testing machine (HUNGTA HT-810, Taichung, Taiwan) was used to load 7, 12, 17, and 22 kg (corresponding stress of 33.01, 56.59, 80.17, and 103.75 kg/mm^2, respectively) to test the strength of the Al-Ni-Cu alloy. The fatigue characteristics of the Al-Ni-Cu alloy were compared with the stress–number (S–N) of cycles to failure curve. The number of cycles to failure was determined by the average of 3–5 rotating fatigue tests for respective heat treatment parameters. Moreover, the fatigue fracture surface was observed through scanning electron microscopy (SEM) to confirm the fracture phenomenon and determine the fracture mechanism.

3. Results and Discussion

3.1. Microstructure Characteristics

Figure 3a,b illustrate the three-dimensional microstructure of the As-printed SLM Al-Ni-Cu alloy, which exhibits a layered melting pool structure. The width and depth of the melting pool are approximately 250 μm and 50–100 μm. Figure 3c,d illustrate the specimen obtained after solution heat treatment at 530 °C for 1 h and aging heat treatment at 175 °C for 6 h (specimen E). The specimen still exhibited an obvious melting pool structure, which indicates that the traditional heat treatment process (530 °C for 1 h and 175 °C for 6 h) [34] did not completely decompose the melting pool structure. Many long grains were parallel to the BD direction in the melting pools (Figure 3d).

Figure 4 displays the XRD analysis results of the As-printed alloy subjected to solution heat treatment at 530 °C for 1 h and aging heat treatment at 175 °C for 6 h. The phase compositions of the As-printed material and powder were almost the same as those in Figure 1, which indicated that the rapid solidification process in SLM did not change the phase composition. In addition to the aluminum matrix, the alloy contained small quantities of precipitation strengthening phases, including $Al_7Cu_{23}Ni$, $AlCu_3$, and Al_3Ni. After heat treatment, no new precipitates were formed. Compared with the As-printed specimen, the quantity of $Al_7Cu_{23}Ni$, $AlCu_3$, and Al_3Ni precipitated in the SLM Al-Ni-Cu alloy increased after heat treatment.

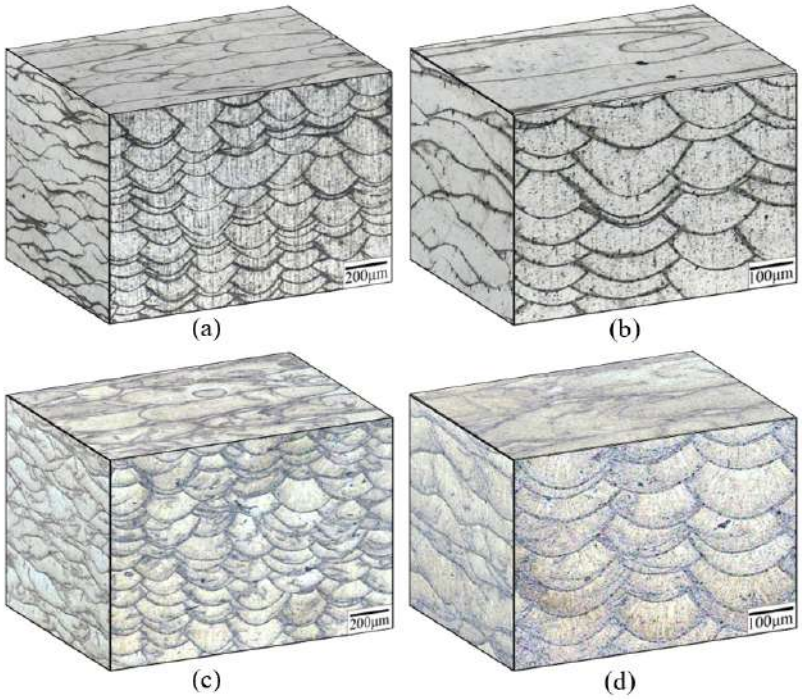

Figure 3. Three-dimensional microstructure of the Al-Ni-Cu alloy: (**a**) As-printed (50×), (**b**) As-printed (100×), (**c**) 530 °C for 1 h and 175 °C for 6 h (50×), and (**d**) 530 °C for 1 h and 175 °C for 6 h (100×).

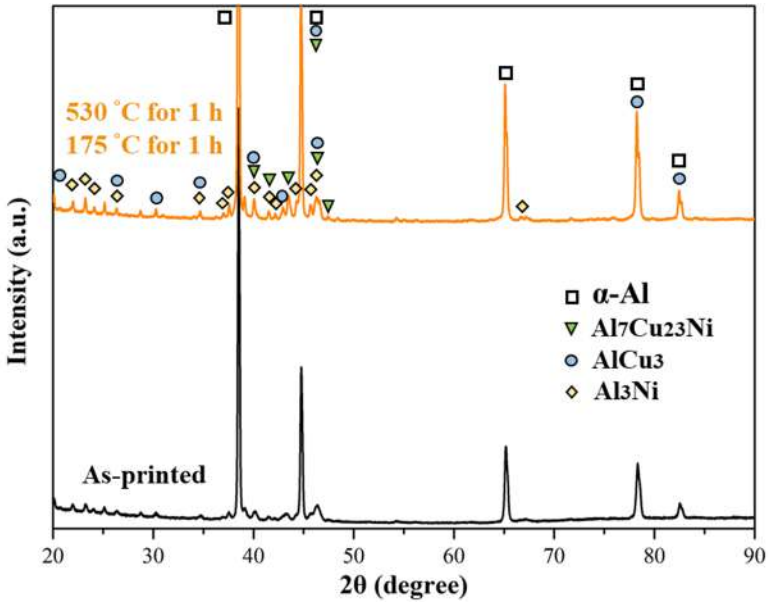

Figure 4. XRD pattern of the Al-Ni-Cu alloy before and after solution treatment.

3.2. Tensile Properties and Hardness

To investigate the influence of the microstructure on the mechanical properties, the hardness and tensile mechanical properties were investigated at room temperature. Figure 5 displays the results of hardness measurement (HRF). No significant difference was observed in the hardness between the As-printed specimen and the specimen obtained after solution heat treatment (530 °C for 1 h) and various aging treatments (175 °C for x h, x = 2, 4, and 6). The hardness was approximately HRF95. This result indicated that the As-printed SLM Al-Ni-Cu alloy had high hardness. The precipitation strengthening effect of $Al_7Cu_{23}Ni$ is less than decreasing of solid solution strengthening, resulting in decreasing in hardness. The trend is the same as research of Gao et al. [35]. Thus, the traditional

heat treatment process could not effectively improve the hardness of the SLM Al-Ni-Cu alloy matrix.

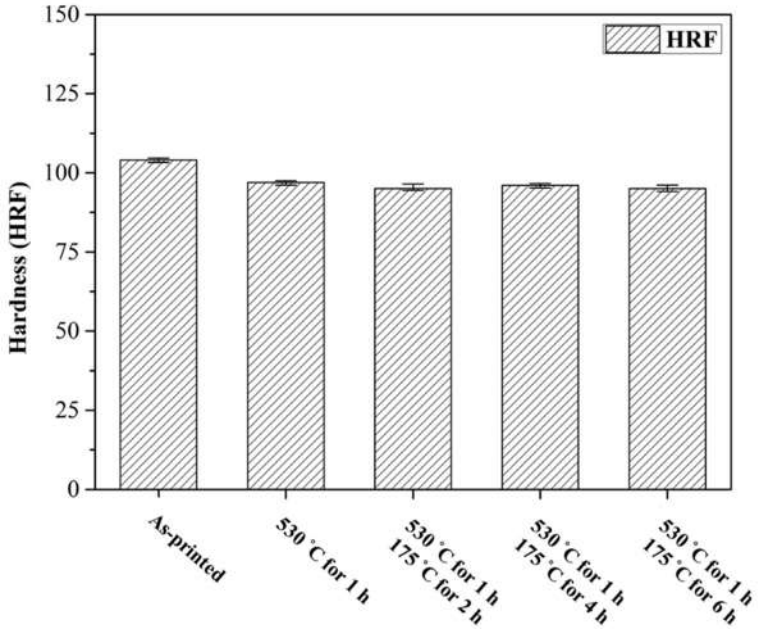

Figure 5. Hardness of the Al-Ni-Cu alloy before and after solution treatment.

Figures 6 and 7 illustrate the macroscopic fracture surface and tensile mechanical properties of the SLM Al-Ni-Cu alloy, respectively, at room temperature. The As-printed (specimen A) Al-Ni-Cu alloy UTS exhibited a mechanical strength of 725 MPa, which is considerably higher than that of other aluminum alloys obtained through SLM and the traditional manufacturing process [9,18,19,21,36]; however, the elongation of the As-printed alloy was only 3.1%. After solution heat treatment (530 °C for 1 h), the strength decreased but the elongation increased considerably. Similar results were obtained after aging (175 °C for x h, x = 2, 4, and 6); however, the strength decreased (UTS: 725 → 550 MPa) and ductility increased (EL: 3% → 10%). Table 4 presents the hardness and mechanical properties of the As-printed specimen and heat-treated specimen. The specimen subjected to solution heat treatment at 530 °C for 1 h and aging heat treatment at 175 °C for 6 h (specimen E) exhibited the best combination of strength and ductility. Therefore, the rotation fatigue characteristics of the As-printed (specimen A) specimen and specimen E were compared. According to previous studies [37,38] and the results illustrated in Figure 3, conventional heat treatment has the following effects on the SLM Al-Ni-Cu alloy structure: (1) local decomposition of the melting pool boundaries, (2) long grains formation in the area of the melting pool, and (3) aggregation of precipitated phases near the boundary of the melting pool. Melting pool structure caused by the rapid cooling in the SLM process can hinder the movement of dislocation and has high strength. Heat treatment locally decomposed the melting pool boundaries, resulting in the easy movement of dislocation. Thus, the SLM Al-Ni-Cu alloy subjected to conventional heat treatment exhibited two mechanical properties: (1) high hardness and reduced residual stress [12] and (2) increased elongation. After traditional heat treatment, the tensile strength decreased; however, excellent strengths of approximately 550 and 370 MPa were maintained for UTS and YS, respectively. The main cause of the texture effect (advantage) at the boundary of the melting pool was that $Al_7Cu_{23}Ni$, $AlCu_3$, and Al_3Ni exhibited nonuniform precipitation (defects).

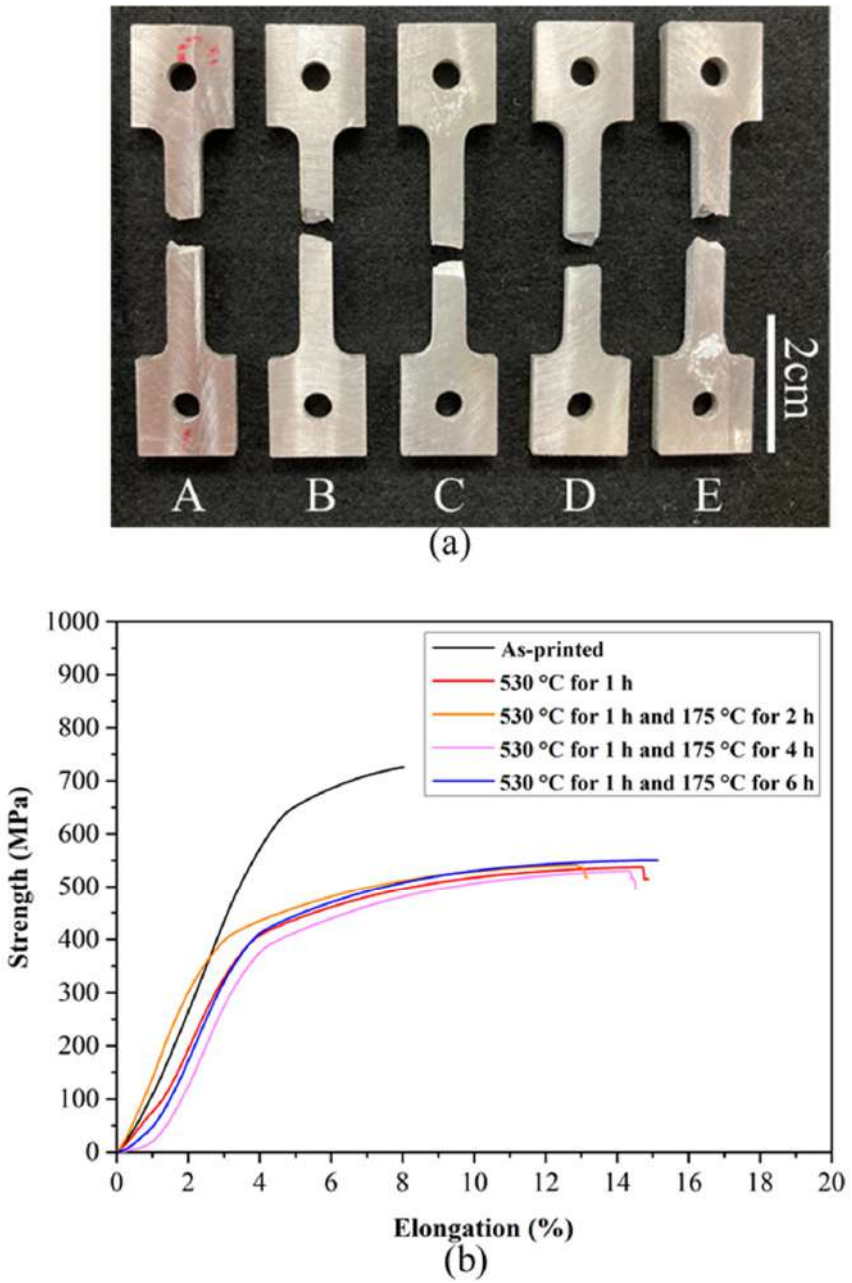

Figure 6. Tensile test of the Al-Ni-Cu alloy before and after solution treatment: (**a**) macroview of the fracture specimen and (**b**) stress–strain curve.

Table 4. Tensile properties and hardness of the Al-Ni-Cu alloy before and after solution treatment.

-	YS (MPa)	UTS (MPa)	UE (%)	TE (%)	HRF
A	578	725	3.1	3.1	104
B	373	537	9.8	10.3	97
C	352	540	9.2	9.7	95
D	376	527	8.9	9.4	96
E	378	550	10.1	10.4	95

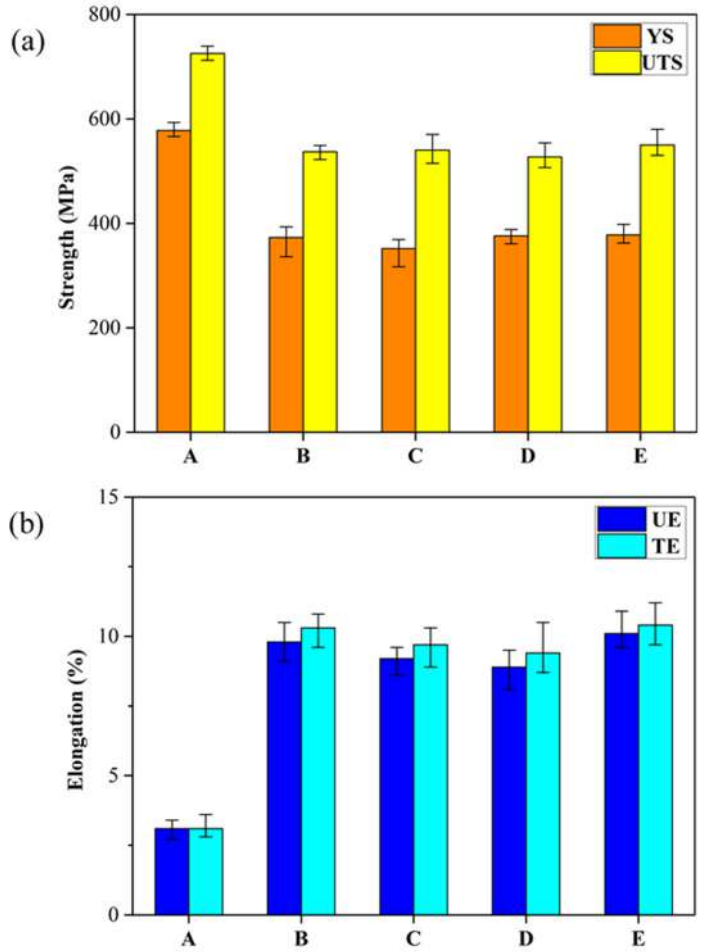

Figure 7. Tensile properties of the Al-Ni-Cu alloy before and after solution treatment: (**a**) strength and (**b**) ductility.

3.3. Fatigue Characteristics

The macrofracture morphology and S–N curve of the As-printed specimen (specimen A) subjected to solution heat treatment at 530 °C for 1 h and aging heat treatment at 175 °C for 6 h (specimen E) are displayed in Figures 8 and 9, respectively. Under various loads, the fracture section of the As-printed specimen was flat without large-area cracks. After heat treatment, the SLM Al-Ni-Cu alloy exhibited a saw-tooth fracture surface (Figure 8). Critically, the fatigue resistance of the SLM Al-Ni-Cu alloy decreased considerably after heat treatment (Figure 9). The fatigue life values are listed in Table 5.

Table 5. Fatigue resistance of the Al-Ni-Cu alloy before and after solution treatment.

Load (kg)	Stress (kg/mm^2)	N (Number of Cycles to Failure)
As-printed		
7	33	26090
12	56.6	4811
17	80.2	4936
22	103.7	2591
530 °C for 1 h and 175 °C for 6 h		
7	33	6767
12	56.6	3754
17	80.2	2436
22	103.7	1204

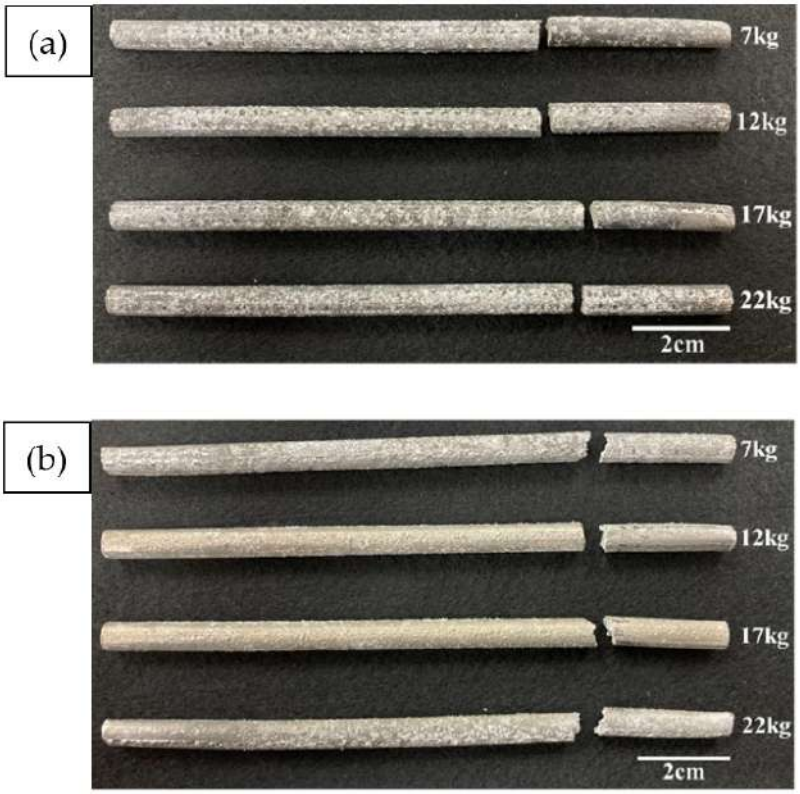

Figure 8. Macroview of the fatigue fracture of the Al-Ni-Cu alloy before and after solution treatment: (**a**) As-printed and (**b**) 530 °C for 1 h and 175 °C for 6 h specimen.

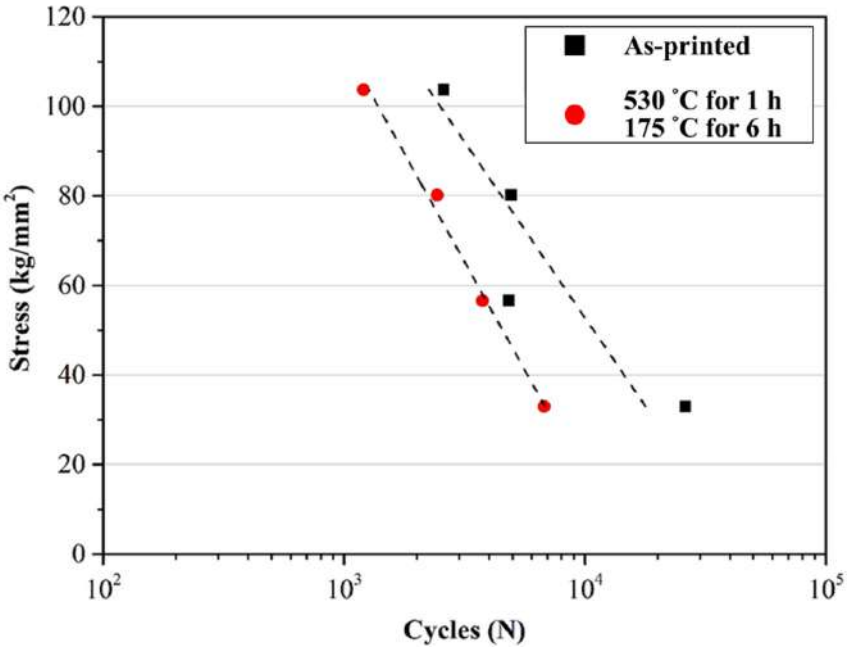

Figure 9. S–N data of the Al-Ni-Cu alloy before and after solution treatment.

Figure 10 displays the characteristics of the fatigue fracture section before and after heat treatment. The difference between the crack propagation region and the final crack region are clearly distinguished from the macrostructure, and both can be observed under SEM; furthermore, the fracture morphology of the two specimens in the two regions differed considerably [39]. The macroscopic fractured section of the As-printed material was flat and had larger undulations after heat treatment. Figure 11a,b display high-

magnification SEM images of the crack propagation region and final crack region of the As-printed specimen, respectively. The crack propagation region is small and exhibits parallel stripes, whereas the final crack region is large and exhibits a wavy dimple fracture morphology. Figure 11c,d display the crack propagation and final crack regions of the heat-treated specimen, respectively. Compared with the As-printed specimen, the specimen obtained after heat treatment had a larger crack propagation region, flatter fracture surface, and a final crack region with less obvious fluctuations. Overall, the heat-treated specimen exhibited brittle fracture characteristics. Notably, the SLM Al-Ni-Cu alloy heat-treated specimen (specimen E) had a tensile elongation of approximately 10% and underwent brittle failure in the fatigue test [40].

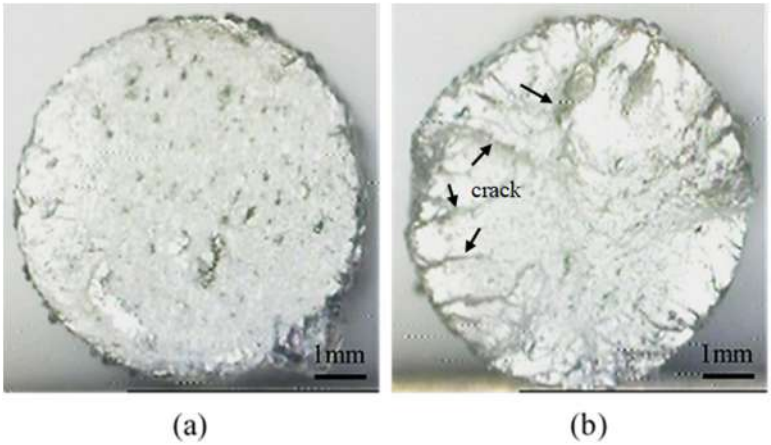

Figure 10. Macrostructure of the fatigue fracture of the Al-Ni-Cu alloy before and after solution treatment (load: 17 kg): (**a**) As-printed and (**b**) 530 °C for 1 h and 175 °C for 6 h.

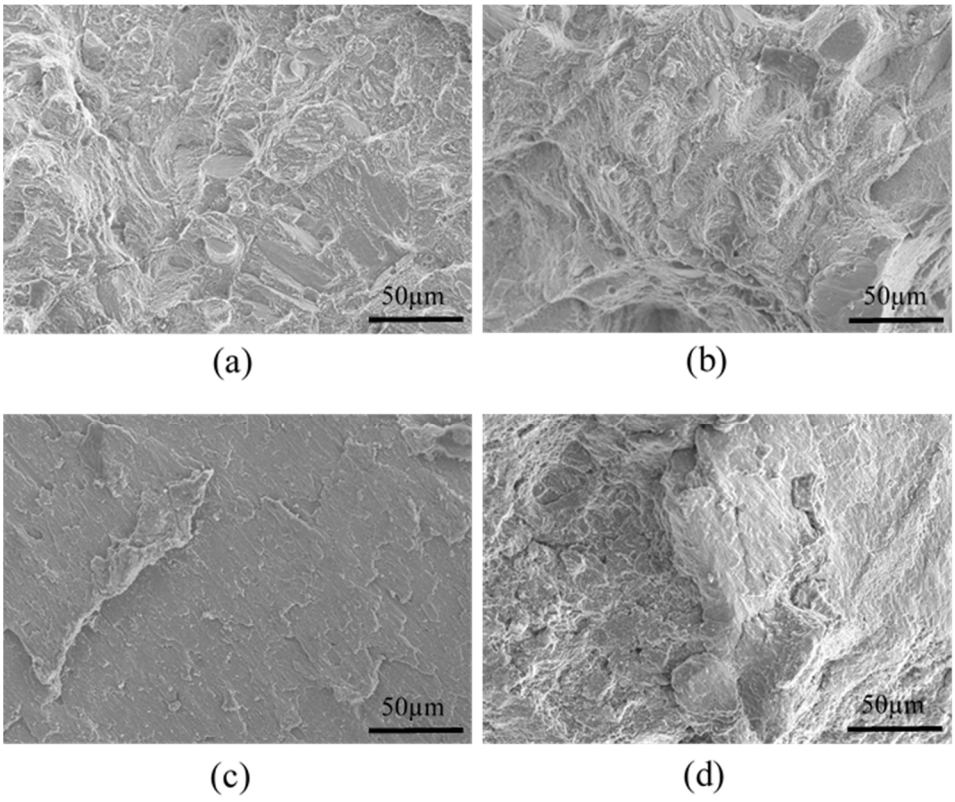

Figure 11. Microstructure of the fatigue fracture of the Al-Ni-Cu alloy before and after solution treatment (load: 17 kg): (**a**) crack propagation region of As-printed, (**b**) final crack region of As-printed, (**c**) crack propagation region of 530 °C for 1 h and 175 °C for 6 h, and (**d**) final crack region of 530 °C for 1 h and 175 °C for 6 h.

$Al_7Cu_{23}Ni$, $AlCu_3$, and Al_3Ni were the precipitation strengthening phases, which increased the ductility of the Al-Ni-Cu alloy and caused it to retain a certain strength after heat treatment. $Al_7Cu_{23}Ni$ precipitated at the junction of the melting pool. According to the XRD results, the peak near 45 degree increased significantly after heat treatment. Combined with the observation of the microstructure, it was inferred that $Al_7Cu_{23}Ni$ was the main strengthening phase and preferentially precipitated at the grain boundary [22,41]. Therefore, $Al_7Cu_{23}Ni$ failed to delay the propagation of fatigue cracks during the fatigue test. The boundary of the original melting pool became the starting point of the fracture that formed a large region of crack propagation, which resulted in a decrease in the fatigue resistance of the specimen after heat treatment. The crack propagation region of the As-printed material was smaller and less susceptible than that of the heat-treated sample was. However, its ductility was poor. The material resisted repeated stress damage due to the original high strength. Thus, the material had superior fatigue resistance. The texture effect of the melting pool before and after heat treatment on tensile failure and fatigue failure is displayed in Figure 12.

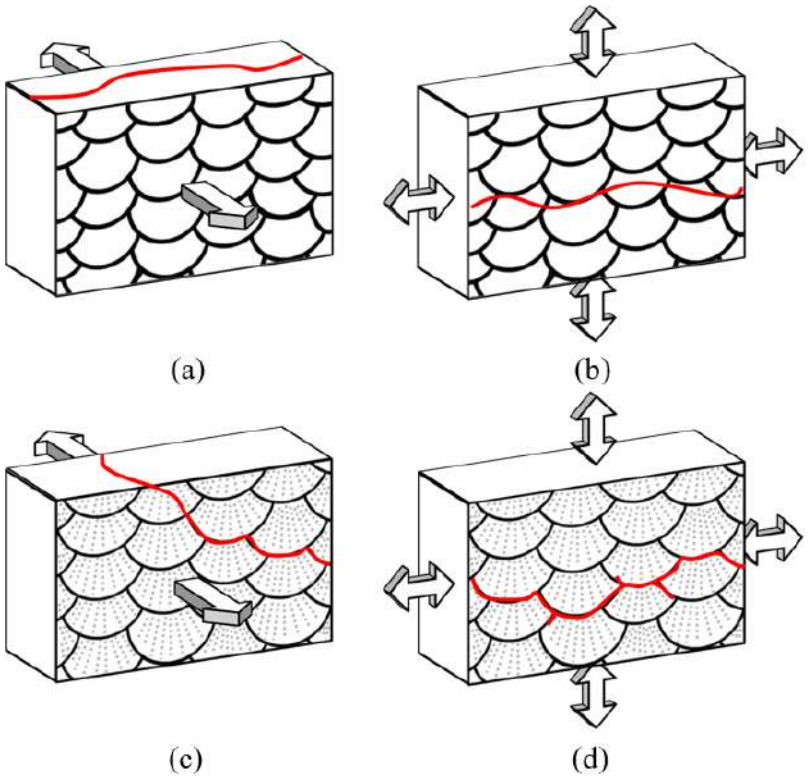

Figure 12. Schematic of the force direction and texture effect before and after heat treatment: (**a**) tensile failure of As-printed, (**b**) fatigue failure of As-printed, (**c**) tensile failure of heat-treated, and (**d**) fatigue failure of heat-treated.

This study confirmed that the alloy subjected to solution heat treatment at 530 °C for 1 h and the aging heat treatment at 175 °C for 6 h was affected by the texture effect and precipitation behavior of the residual melting pool boundary, which reduced the fatigue life of the alloy. The As-printed material exhibited a high yield strength. Although its ductility was low, the aforementioned material still exhibited a high fatigue life. Therefore, this system should deviate from the conventional aluminum alloy heat treatment conditions and have higher solution temperature and reaction time. The modified conditions caused the melting pool structure to completely disappear. Thus, uniform precipitation strengthening can be used to expand the applicability of SLM Al-Ni-Cu alloys.

4. Conclusions

1. The SLM Al-Ni-Cu alloy exhibited typical melting pool stacking characteristics. The base contained $Al_7Cu_{23}Ni$, $AlCu_3$, and Al_3Ni precipitates, and the tensile mechanical properties of the aforementioned alloy, were superior to those of conventionally cast Al-Ni alloys.

2. The heat treatment process caused the partial decomposition of the melting pool boundary in the SLM Al-Ni-Cu alloy structure. Long grains were formed in the melting pool area, and the precipitated phases aggregated near the melting pool boundary. Therefore, the tensile strength decreased and the elongation considerably increased.

3. Heat treatment promoted $Al_7Cu_{23}Ni$ precipitation at the boundary of the Al-Ni-Cu alloy melting pool. A texture effect still existed at the boundary of the melting pool, which resulted in the heat-treated SLM Al-Ni-Cu alloy exhibiting excellent elongation and brittle fatigue failure.

Author Contributions: Methodology, K.-C.C.; investigation, K.-C.C.; data curation, K.-C.C.; writing—original draft preparation, K.-C.C.; writing—review and editing, J.-R.Z. and F.-Y.H.; supervision, J.-R.Z. and F.-Y.H. All authors have read and agreed to the published version of the manuscript.

Funding: This research received no external funding.

Institutional Review Board Statement: Not applicable.

Informed Consent Statement: Not applicable.

Data Availability Statement: The data presented in this study are available on request from the corresponding author. The data are not publicly available due to privacy or ethics.

Acknowledgments: The authors are grateful to the Instrument Center of National Cheng Kung University and the Ministry of Science and Technology of Taiwan (Grant No. MOST 108-2221-E-006-140-MY3) for their financial support. They thank the Taiwan Circle Metal Powder Co., Ltd. and Taiwan ANJI Technology Co., Ltd. for providing the alloy powder and SLM printer, respectively.

Conflicts of Interest: The authors declare no conflict of interest.

References

1. Osório, W.R.; Peixoto, L.C.; Cante, M.V.; Garcia, A. Microstructure features affecting mechanical properties and corrosion behavior of a hypoeutectic Al–Ni alloy. *Mater. Des.* **2010**, *31*, 4485–4489. [CrossRef]
2. Fan, Y.; Makhlouf, M.M. The effect of introducing the Al–Ni eutectic composition into Al–Zr–V alloys on microstructure and tensile properties. *Mater. Sci. Eng. A* **2016**, *654*, 228–235. [CrossRef]
3. Suwanpreecha, C.; Pandee, P.; Patakham, U.; Limmaneevichitr, C. New generation of eutectic Al-Ni casting alloys for elevated temperature services. *Mater. Sci. Eng. A* **2018**, *709*, 46–54. [CrossRef]
4. Zhuang, Y.; Zhang, X.; Zhu, L.; Hu, Z. Eutectic spacing and faults of directionally solidified Al–Al3Ni eutectic. *Sci. Technol. Adv. Mater.* **2001**, *2*, 37–39. [CrossRef]
5. Uan, J.; Chen, L.; Lui, T. On the extrusion microstructural evolution of Al–Al3Ni in situ composite. *Acta Mater.* **2001**, *49*, 313–320. [CrossRef]
6. Zhang, Z.-G.; Watanabe, Y.; Kim, I. Effect of texture evolution on tensile properties of Al–Ni eutectic alloy fabricated by equal channel angular pressing. *Mater. Sci. Technol.* **2005**, *21*, 708–714. [CrossRef]
7. Spinelli, J.E.; Cante, M.V.; Cheung, N.; Mangelinck-Noël, N.; Garcia, A. SEM Characterization of Al3Ni Intermetallics and its Influence on Mechanical Properties of Directionally Solidified Hypoeutectic Al-Ni Alloys. *Mater. Sci. Forum* **2010**, *636*, 465–470. [CrossRef]
8. Srivastava, N.; Chaudhari, G.P. Effect of ultrasonic treatment on the mechanical behaviour of Al–Ni alloys. *Mater. Sci. Technol.* **2019**, *35*, 1239–1247. [CrossRef]
9. Peng, P.; Zhang, A.; Yue, J. Competitive growth of leading phase and tensile properties of directionally solidified eutectic Al–Ni alloy. *Mater. Sci. Eng. A* **2020**, *773*, 138887. [CrossRef]
10. Zhao, J.-R.; Hung, F.-Y.; Lui, T.-S.; Wu, Y.-L. The Relationship of Fracture Mechanism between High Temperature Tensile Mechanical Properties and Particle Erosion Resistance of Selective Laser Melting Ti-6Al-4V Alloy. *Metals* **2019**, *9*, 501. [CrossRef]
11. Zhao, J.R.; Hung, F.Y.; Lui, T.S. Microstructure and tensile fracture behavior of three-stage heat treated inconel 718 alloy produced via laser powder bed fusion process. *J. Mater. Res. Technol.* **2020**, *9*, 3357–3367. [CrossRef]
12. Chen, K.-J.; Hung, F.-Y.; Lui, T.-S.; Tsai, C.-L. Improving the applicability of wear-resistant Al–10Si–0.5 Mg alloy obtained through selective laser melting with T6 treatment in high-temperature, and high-wear environments. *J. Mater. Res. Technol.* **2020**, *9*, 9242–9252. [CrossRef]

13. Sun, J.; Yang, Y.; Wang, D. Parametric optimization of selective laser melting for forming Ti6Al4V samples by Taguchi method. *Opt. Laser Technol.* **2013**, *49*, 118–124. [CrossRef]
14. Do, D.K.; Li, P. The effect of laser energy input on the microstructure, physical and mechanical properties of Ti-6Al-4V alloys by selective laser melting. *Virtual Phys. Prototyp.* **2016**, *11*, 41–47. [CrossRef]
15. Rickenbacher, L.; Etter, T.; Hovel, S.; Wegener, K. High temperature material properties of IN738LC processed by selective laser melting (SLM) technology. *Rapid Prototyp. J.* **2013**, *19*, 282–290. [CrossRef]
16. Yan, Q.; Song, B.; Shi, Y. Comparative study of performance comparison of AlSi10Mg alloy prepared by selective laser melting and casting. *J. Mater. Sci. Technol.* **2020**, *41*, 199–208. [CrossRef]
17. Ch, S.R.; Raja, A.; Jayaganthan, R.; Vasa, N.; Raghunandan, M. Study on the fatigue behaviour of selective laser melted AlSi10Mg alloy. *Mater. Sci. Eng. A* **2020**, *781*, 139180. [CrossRef]
18. Yu, Y.; Yu, J.J.; Zhang, H.; Zhao, H.B.; Nie, D.R.; Xiao, B.L.; Ma, Z.X. Effects of Heat Treatments on Microstructure and Me-chanical Properties of AlSi10Mg Alloy Produced by Selective Laser Melting. *Acta. Metall. Sin.* **2020**.
19. Shi, Y.; Yang, K.; Kairy, S.K.; Palm, F.; Wu, X.; Rometsch, P.A. Effect of platform temperature on the porosity, microstructure and mechanical properties of an Al–Mg–Sc–Zr alloy fabricated by selective laser melting. *Mater. Sci. Eng. A* **2018**, *732*, 41–52. [CrossRef]
20. Spierings, A.; Dawson, K.; Dumitraschkewitz, P.; Pogatscher, S.; Wegener, K. Microstructure characterization of SLM-processed Al-Mg-Sc-Zr alloy in the heat treated and HIPed condition. *Addit. Manuf.* **2018**, *20*, 173–181. [CrossRef]
21. Ma, R.; Peng, C.; Wang, R.; Wang, R.; Zhou, Z.; Li, X.; Cao, X. Effect of bimodal microstructure on the tensile properties of selective laser melt Al-Mg-Sc-Zr alloy. *J. Alloy. Compd.* **2020**, *815*, 152422. [CrossRef]
22. Sun, S.; Liu, P.; Hu, J.; Hong, C.; Qiao, X.; Liu, S.; Zhang, R.; Wu, C. Effect of solid solution plus double aging on microstructural characterization of 7075 Al alloys fabricated by selective laser melting (SLM). *Opt. Laser Technol.* **2019**, *114*, 158–163. [CrossRef]
23. Liu, P.; Hu, J.-Y.; Li, H.-X.; Sun, S.-Y.; Zhang, Y.-B. Effect of heat treatment on microstructure, hardness and corrosion resistance of 7075 Al alloys fabricated by SLM. *J. Manuf. Process.* **2020**, *60*, 578–585. [CrossRef]
24. Chen, X.; Liu, K.; Guo, W.; Gangil, N.; Siddiquee, A.N.; Konovalov, S. The fabrication of NiTi shape memory alloy by selective laser melting: A review. *Rapid Prototyp. J.* **2019**, *25*, 1421–1432. [CrossRef]
25. Konovalov, S.; Osintsev, K.; Golubeva, A.; Smelov, V.; Ivanov, Y.; Chen, X.; Komissarova, I. Surface modification of Ti-based alloy by selective laser melting of Ni-based superalloy powder. *J. Mater. Res. Technol.* **2020**, *9*, 8796–8807. [CrossRef]
26. Zhang, L.-C.; Attar, H. Selective Laser Melting of Titanium Alloys and Titanium Matrix Composites for Biomedical Applications: A Review. *Adv. Eng. Mater.* **2016**, *18*, 463–475. [CrossRef]
27. Boussinot, G.; Döring, M.; Hemes, S.; Stryzhyboroda, O.; Apel, M.; Schmidt, M. Laser powder bed fusion of eutectic Al–Ni alloys: Experimental and phase-field studies. *Mater. Des.* **2021**, *198*, 109299. [CrossRef]
28. Churyumov, A.Y.; Pozdniakov, A.V.; Prosviryakov, A.; Loginova, I.S.; Daubarayte, D.K.; Ryabov, D.; A Korolev, V.; Solonin, A.N.; Pavlov, M.D.; Valchuk, S.V. Microstructure and mechanical properties of a novel selective laser melted Al–Mg alloy with low Sc content. *Mater. Res. Express* **2019**, *6*, 126595. [CrossRef]
29. Knoop, D.; Lutz, A.; Mais, B.; Von Hehl, A. A Tailored AlSiMg Alloy for Laser Powder Bed Fusion. *Metals* **2020**, *10*, 514. [CrossRef]
30. Li, J.; Birbilis, N.; Li, C.; Jia, Z.; Cai, B.; Zheng, Z. Influence of retrogression temperature and time on the mechanical properties and exfoliation corrosion behavior of aluminium alloy AA7150. *Mater. Charact.* **2009**, *60*, 1334–1341. [CrossRef]
31. Kim, J.; Jeong, H.; Hong, S.; Kim, Y.; Kim, W. Effect of aging treatment on heavily deformed microstructure of a 6061 aluminum alloy after equal channel angular pressing. *Scr. Mater.* **2001**, *45*, 901–907. [CrossRef]
32. Li, Y.; Brusethaug, S.; Olsen, A. Influence of Cu on the mechanical properties and precipitation behavior of AlSi7Mg0.5 alloy during aging treatment. *Scr. Mater.* **2006**, *54*, 99–103. [CrossRef]
33. Li, J.-F.; Huang, J.-L.; Liu, D.-Y.; Chen, Y.-L.; Zhang, X.-H.; Ma, P.-C. Distribution and evolution of aging precipitates in Al-Cu-Li alloy with high Li concentration. *Trans. Nonferrous Met. Soc. China* **2019**, *29*, 15–24. [CrossRef]
34. Boonchouytan, W.; Chatthong, J.; Rawangwong, S.; Burapa, R. Effect of Heat Treatment T6 on the Friction Stir Welded SSM 6061 Aluminum Alloys. *Energy Procedia* **2014**, *56*, 172–180. [CrossRef]
35. Gao, C.; Liu, Z.; Xiao, Z.; Zhang, W.; Wong, K.; Akbarzadeh, A. Effect of heat treatment on SLM-fabricated TiN/AlSi10Mg composites: Microstructural evolution and mechanical properties. *J. Alloy. Compd.* **2021**, *853*, 156722. [CrossRef]
36. Campbell, F.C. Elements of Metallurgy and Engineering Alloys. *ASM Int.* **2008**, *26*, 487–508.
37. Fan, Y.; Makhlouf, M.M. The Al-Al3Ni Eutectic Reaction: Crystallography and Mechanism of Formation. *Met. Mater. Trans. A* **2015**, *46*, 3808–3812. [CrossRef]
38. Zuo, L.; Ye, B.; Feng, J.; Zhang, H.; Kong, X.; Jiang, H. Effect of ε-Al3Ni phase on mechanical properties of Al–Si–Cu–Mg–Ni alloys at elevated temperature. *Mater. Sci. Eng. A* **2020**, *772*, 138794. [CrossRef]
39. Xia, F.; Gao, X.; Liang, M.; Guo, Y.; Li, J.; Yang, Z.; Wang, J.; Zhang, L. Effect of thermal exposure on microstructure and high-temperature fatigue life of Al-Si piston alloys. *J. Mater. Res. Technol.* **2020**, *9*, 12926–12935. [CrossRef]
40. Xue, Y.; El Kadiri, H.; Horstemeyer, M.F.; Jordon, J.B.; Weiland, H. Micromechanisms of multistage fatigue crack growth in a high-strength aluminum alloy. *Acta Mater.* **2007**, *55*, 1975–1984. [CrossRef]
41. Mohammadi, A.; Enikeev, N.; Murashkin, M.Y.; Arita, M.; Edalati, K. Developing age-hardenable Al-Zr alloy by ultra-severe plastic deformation: Significance of supersaturation, segregation and precipitation on hardening and electrical conductivity. *Acta Mater.* **2021**, *203*, 116503. [CrossRef]